Eur. Phys. J. Special Topics **224**, 25–34 (2015)

DOI: 10.1140/epjst/e2015-02340-6

THE EUROPEAN PHYSICAL JOURNAL SPECIAL TOPICS

Review

Quantum tunneling vs. thermal effects in experiments on adiabatic quantum computing

D.M. Silevitch[1], T.F. Rosenbaum[1,2,a] and G. Aeppli[3,4,5]

[1] The James Franck Institute and Department of Physics, The University of Chicago, Chicago, Illinois 60637, USA
[2] Division of Physics, Mathematics and Astronomy, California Institute of Technology, Pasadena, California 91125, USA
[3] Departments of Physics, Swiss Federal Institutes of Technology, Zurich and Lausanne, Switzerland
[4] Paul Scherrer Institute, Villigen, Switzerland
[5] London Centre for Nanotechnology and Department of Physics and Astronomy, UCL, London WC1E 6BT, UK

Received 19 September 2014 / Received in final form 16 December 2014

Abstract. Traditional simulated annealing uses thermal fluctuations for convergence in optimization problems. Quantum tunneling provides a different mechanism for moving between states, with the potential for reduced time scales and different outcomes. Thermal and quantum annealing are compared in two concentration regimes of a model disordered magnet, where the effects of quantum mechanics can be tuned both by varying an applied magnetic field and by controlling the strength of thermal coupling between the magnet and an external heat bath. The results indicate that quantum annealing hastens convergence to the final state, and that the quantum character of the final state can be engineered thermodynamically.

1 Introduction

Many complex problems are difficult and slow to solve using conventional computers and over the last several years research towards developing quantum computation has grown steadily. In particular, optimization problems such as the traveling salesman problem, in which the shortest possible route between a number of towns, visiting each once and returning to the point of origin must be determined, becomes intractable as the number of nodes (e.g. towns) grow. A quantum computer has the potential to exploit effects such as entanglement and tunneling that appear on the atomic and molecular size scales to solve such problems dramatically faster than conventional computers [1–5].

Recently, a first generation of specialized computers has become available, with a new architecture that exploits quantum mechanics to help solve traveling salesman problems with up to a few hundred towns [5]. We describe in this chapter the

---

[a] e-mail: tfr@caltech.edu

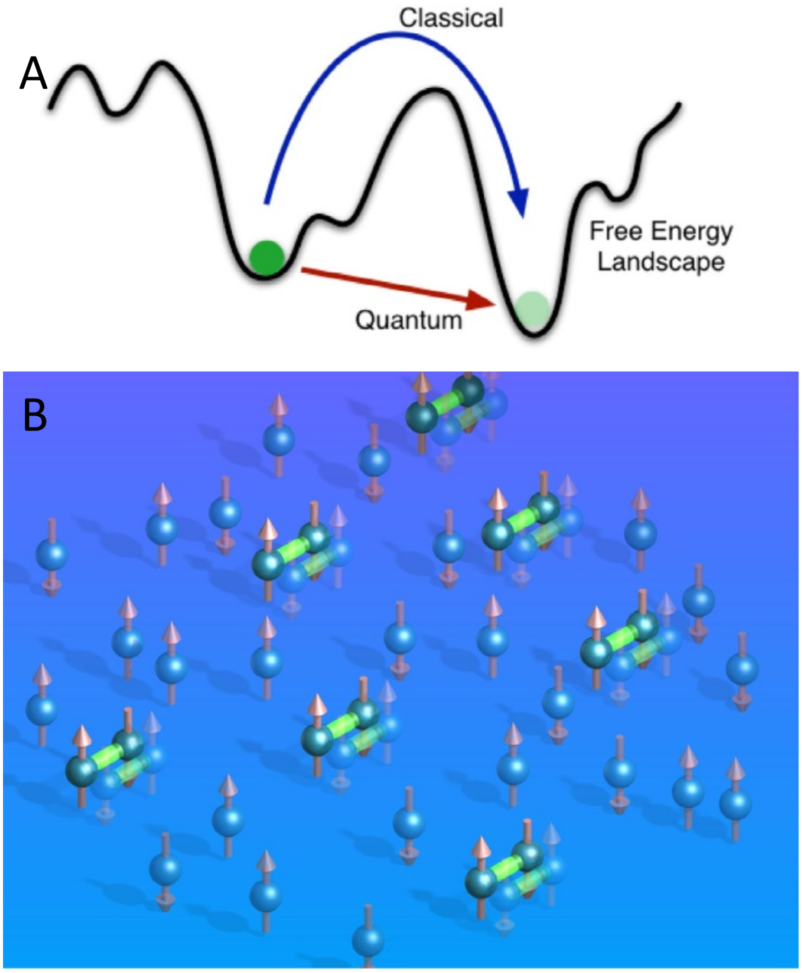

Fig. 1. Overview of quantum annealing in $LiHoYF_4$. A) Schematic of free energy landscape showing transitions mediated by thermal excitation (classical) and transverse-field induced tunneling (quantum). B) Representation of final state of $LiHo_{0.045}Y_{0.955}F_4$ after a quantum annealing protocol. Some fraction of the spins form tight-bound states with adjoining spins, in quantum superpositions of the underlying eigenstates.

harnessing of a bulk quantum magnet, a crystal containing a thermodynamic number N, rather than hundreds, of quantum mechanical spins, to understand the $N \rightarrow \infty$ limit of the current generation of much smaller specialized computers.

One of the key aspects of optimization is the process by which the special purpose computer settles into a solution to problems like that of the traveling salesman. The solutions to the problem exist in a landscape where the heights and depths of features are the total distance traveled – the best solution corresponds to the deepest valley. To find the deepest valley, the optimizer hops between valleys either by climbing to intermediate saddle points and then descending again, or via quantum tunneling between valleys (Fig. 1A). The first represents thermal annealing, while the second corresponds to quantum annealing. The relative weights of the thermal and quantum processes determine the nature of the final valley found.

Our experiments on the crystalline magnetic salt, Li(Ho, Y)F_4, look at the valleys found after annealing with different rations of weights [6–8]. In this material, at temperatures near absolute zero, the speed and strength of thermal annealing can be controlled by rods of sapphire attached to a refrigerator with more or less contact with the crystal [8]. At the same time, the rate of quantum annealing can be controlled by means of a magnetic field that acts to set the rate of quantum tunneling in the sample [7].

We found that when the system reached its final valley via thermal annealing alone, it was dramatically different from the state reached when the thermal annealing was weakened and quantum annealing was turned on. Figure 1B is a schematic of the state found after quantum annealing, where certain regions of the crystal are in quantum superposition states and others have definite classical characteristics, marked by fixed up or down arrows; classical annealing of the same system leaves behind regions of exclusively the latter variety. Applied to practical and programmable quantum optimization computers [9], the results imply that quantum optimizers could obtain very different types of solutions to problems such as the traveling salesman problem when compared with conventional annealing techniques, a finding that will affect both the design and use of quantum optimization systems.

2 Background

The experimental system used to investigate the rate of convergence and the ultimate end state under different annealing protocols is Li(Ho, Y)F_4. In these rare-earth fluoride crystals, the magnetism is carried by the Ho^{3+} ions, where the crystal fields induce a ground state doublet and the Ho spins can be modeled as dipole-coupled $S = 1/2$ Ising spins, with the Ising axis oriented along the crystalline c axis (Fig. 2A). The parent compound, $LiHoF_4$, is a ferromagnet with a Curie temperature $T_C = 1.53\,\mathrm{K}$ [10]. Introduction of a magnetic field transverse to the Ising axis splits the ground-state doublet (Fig. 2B) and introduces an S_x term to the Hamiltonian [11,12], giving

$$\hat{H} = -J \sum S_i^z S_j^z - \Gamma \sum S_i^x . \tag{1}$$

This has the effect of coupling the S^z eigenstates with a tunneling rate that is proportional to Γ [13]. In pure $LiHoF_4$, the phase diagram arising from this Transverse Field Ising Model Hamiltonian can be accurately described using mean-field theory [14]; however, the controlled dilution of the magnetism results in behavior beyond the predictions of the mean-field theory [15].

The dilution of the magnetism is realized via site random chemical substitution of non-magnetic yttrium for the magnetic holmium atoms. For large x in $LiHo_xY_{1-x}F_4$, the system retains the possibility of ferromagnetic ordering, with a T_C that is suppressed with decreasing x (Fig. 2C) [16]. In this concentration regime, internal transverse fields arising from the uncompensated nature of the dipole interaction when there is compositional disorder create an effective random-field term in the Hamiltonian [17,18] that pulls the phase boundary below the mean-field prediction (Fig. 2D). For $x < 0.3$, long-range ferromagnetic ordering is no longer stable, and the system can be found in spin glass [19], spin liquid [20], or effectively decoupled spin states [21,22] as x approaches zero (Fig. 2C) [16]. In this Chapter, we will discuss classical and quantum annealing experiments for the dilute ferromagnet ($x = 0.44$) (Refs. [6] and [7]) and the spin glass/liquid ($x = 0.045$) (Ref. [8]) concentrations.

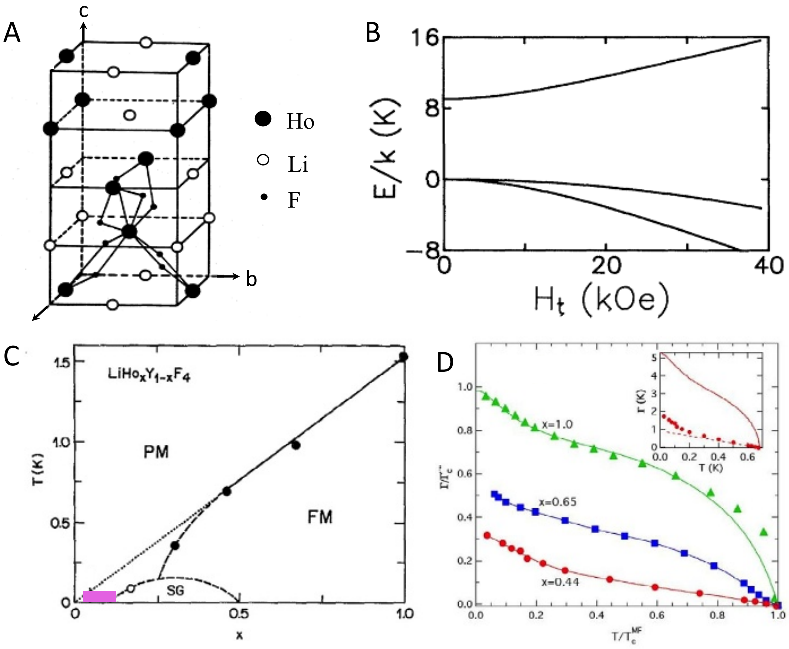

Fig. 2. Structure and static states of LiHoYF$_4$. A) Chemical structure of the parent compound LiHoF$_4$. Magnetic Ho^{3+} ions may be replaced by nonmagnetic Y ions to dilute the magnetism without changing the physical structure. The magnetic Ising axis lies parallel to the crystalline c axis. From Ref. [16]. B) Energy levels of a single Ho^{3+} ion as a function of magnetic field transverse to the Ising axis. The magnetic field lifts the 2-fold degeneracy of the ground state. From Ref. [13]. C) Zero-field magnetic ordering in LiHo$_x$Y$_{1-x}$F$_4$. For large x, the ground state is ferromagnetic with T_C suppressed relative to the parent compound. At smaller x, spin-glass ordering is observed. At $x \sim 5\%$ (shaded rectangle), controlling the thermal boundary conditions can tune the state between a spin glass and a spin liquid. Adapted from Ref. [16]. D) Transverse-field dependence of the ferromagnet-paramagnet phase boundary in ferromagnetic LiHo$_x$Y$_{1-x}$F$_4$. For the parent compound, mean-field theory accurately describes the shape of the phase boundary. In the presence of dilution and finite transverse field, random-field effects suppress the phase boundary compared to the mean-field expectation. From Ref. [15].

3 Results

We first establish that a quantum tunneling picture is an appropriate way of understanding the low temperature relaxation in the disordered ferromagnet, and then compare the results of preparing the system via classical and quantum annealing trajectories. We start by using the frequency-dependent ac magnetic susceptibility to identify an activation frequency f_0 and then examine how this activation frequency changes as a function of temperature and transverse field. As shown in Fig. 3A, below approximately 50 mK, the activation frequency is essentially independent of temperature and instead is primarily tuned by the rate of quantum tunneling as set by the transverse field energy scale Γ. Cuts in Γ at fixed T can be fit to a WKB form, thereby providing a quantitative measure of the domain wall tunneling [7].

We now compare the results of preparing the system via predominantly classical versus predominantly quantum mechanical annealing trajectories as sketched in Fig. 3B [6]. The classical annealing trajectory begins at high temperature and cools in zero transverse field (and hence is dominated by thermal activation over free energy

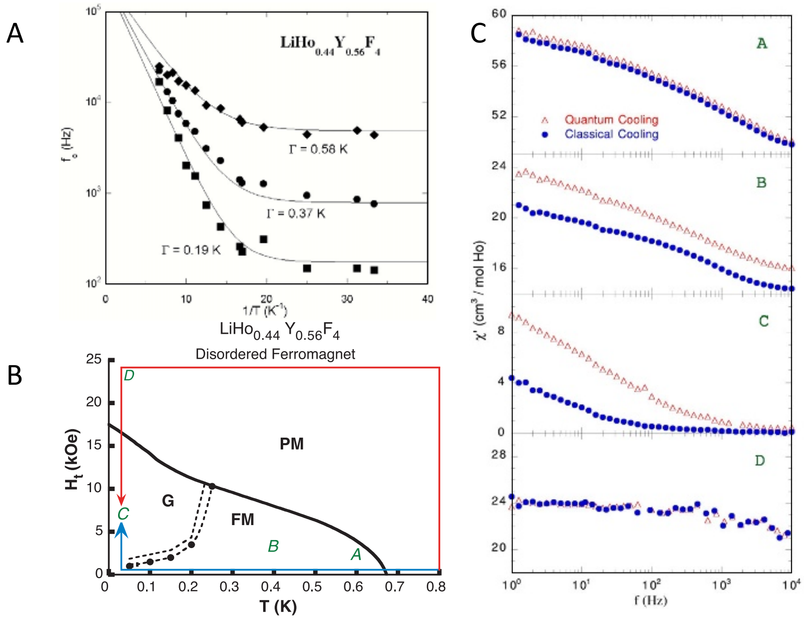

Fig. 3. Quantum and classical annealing in ferromagnetic $\mathrm{LiHo_{0.44}Y_{0.56}F_4}$. A) Activation frequency f_0 as a function of temperature and transverse field. At temperatures below 50 mK, activation rates are primarily dependent on the transverse-field induced tunneling rates rather than temperature, indicating a crossover to a quantum-mechanical dominated regime. (From Ref. [7]) B) Annealing protocols. Starting at 0 transverse field and at T = 675 mK (above the 600 mK Curie temperature), the classical annealing protocol cools in 0 field to the final temperature (marked by points A, B, and C on the graph), and then the transverse field is ramped to the final value. The quantum annealing protocol starts at the same location, ramps the transverse field to 24 kOe, cools to the final temperature, and finally ramps the field down to the final value. (From Ref. [6]) C) Path dependence of system state. For final temperatures near the Curie temperature, there is little apparent difference between cooling paths. At successively lower temperatures, classical vs. quantum cooling paths produce increasingly different final states. For final states in transverse fields large enough to remain in the paramagnet, the annealing trajectory no longer has an effect on the final state. (From Ref. [6].)

barriers). Once low temperature is reached and the system has settled into a local minimum, the transverse field is applied. This is compared to a quantum-annealing trajectory in which the transverse field is first ramped to a large value, the system is cooled in the presence of this large field enabling quantum tunneling through the free energy surface, and finally the field is ramped down to an intermediate value. As can be seen from Fig. 3C, the classical and quantum annealing trajectories yield similar results at elevated temperatures, but as the temperature is dropped, the two trajectories yield increasingly different spectra, indicating that the sample is ending up in a different state depending on which annealing protocol is followed. The quantum annealing protocol is more efficient than thermal annealing at uncovering the $\log(f)$ behavior of $\chi'(f)$ in the final state and approaches that state more quickly, aided by the tunneling of blocks of spins. As expected, when the transverse field is large enough to completely suppress the (marginally stable) ordered state, the paramagnetic ground state becomes insensitive to the annealing protocol.

An alternative approach to varying the relative importance of quantum and thermal annealing is to change the thermal boundaries of the system, as described recently

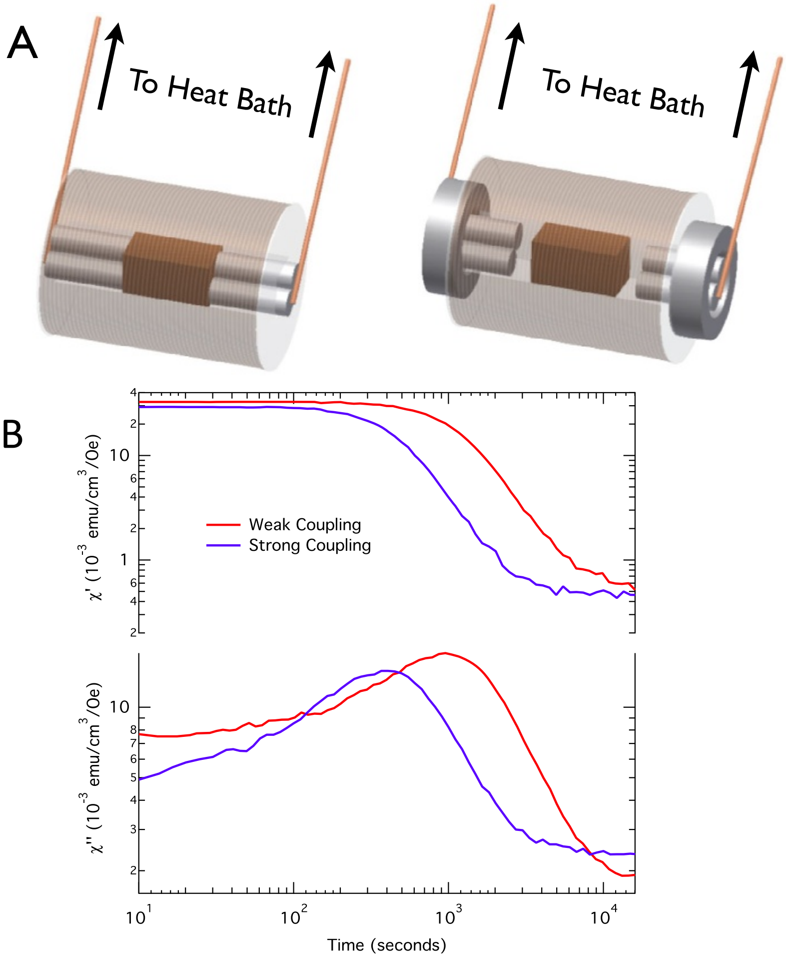

Fig. 4. State tuning in $\mathrm{LiHo_{0.045}Y_{0.955}F_4}$ via control of thermal boundary conditions. (Ref. [8]) A) Experimental apparatus. The sample sits at the center of the coils of a magnetic susceptometer. The primary mode of thermal coupling between the sample and the cryostat heat bath is via sapphire rods pressed against end faces of the sample; the rods are connected via copper wires to the cryostat. To weaken the thermal coupling between the heat bath and the sample, the rods are withdrawn by 4 mm by imposing spacers at the ends. B) Time evolution of the complex ac magnetic susceptibility for the two coupling limits at 90 mK immediately following rapid thermal quenches from 9 K. The different end values of the susceptibility, along with the qualitatively different shapes of the equilibration curves, demonstrate that changing the thermal coupling changes the nature of the final state rather than simply changing the equilibrium temperature.

in Ref. [8]. This experiment, carried out on dilute $\mathrm{LiHo_{0.045}Y_{0.955}F_4}$, is sketched in Fig. 4A. The crystal starts out with a strong thermal connection to the cryostat heat bath via sapphire rods firmly pressed against the end faces of the crystal. This is then contrasted to the behavior of the crystal when the sapphire rods are withdrawn by a few millimeters and contact is solely through an organic resin, significantly reducing the thermal coupling and hence the rate at which heat can flow between the sample and the heat bath. We plot in Fig. 4B the time evolution of the complex susceptibility after a rapid thermal quench from 9 K to 90 mK; as can be seen in the long-time limit,

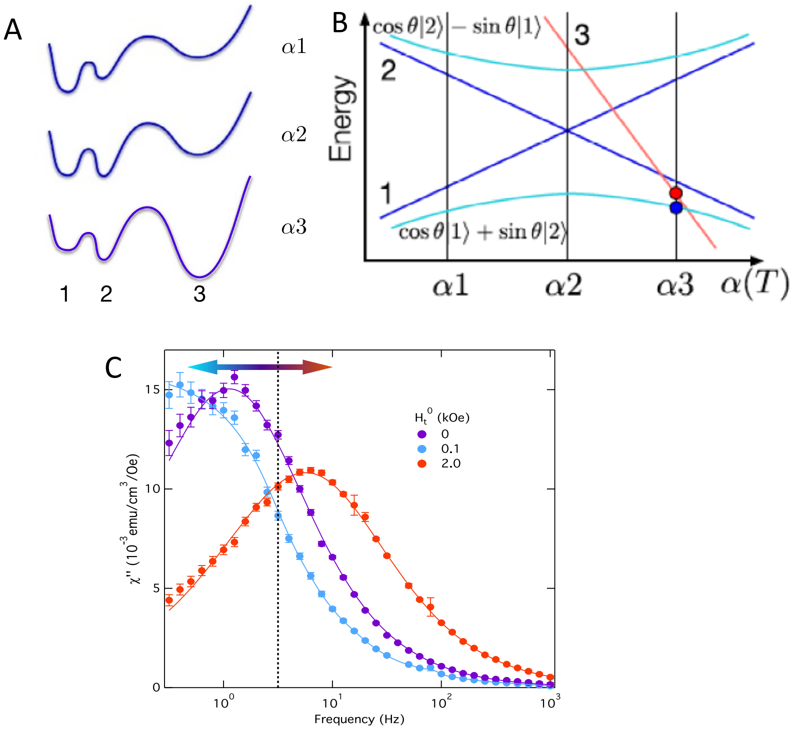

Fig. 5. Using quantum annealing to control the final state in LiHo$_0$.045Y$_{0.955}$F$_4$. (Ref. [8]) A) Schematic showing the thermal evolution (associated with the mean field from other clusters) of the potential energy for different states of a typical spin cluster. B) Quantum mixing of states alters the outcome of the cooling process, with a quantum mixture of eigenstates 1 and 2 rather than the lowest energy state 3 emerging for cooling rapid compared to decoherence rates. C) Imaginary susceptibility of LiHo$_0$.045Y$_{0.955}$F$_4$ with weak coupling to the bath after cooling from 9 to 0.09 K in a transverse field H_t^0. The spectrum moves non-monotonically with H_t^0, first slowing from enhanced random field pinning and then moving to higher frequency via transverse field-induced tunneling. Dashed line at 3.1 Hz indicates constant-frequency cut used in Fig. 6.

changing the thermal boundary conditions changes the final state. There are multiple crossings of the imaginary susceptibility traces, showing that the weak-coupling limit is not simply a slowly-cooled, delayed, variant of the strong-coupling case (if that were true, the weak-coupling trace would be a stretched version of the strong-coupling), but instead is a qualitatively different state with a quantitatively different asymptote.

In the weak-coupling regime, where thermal effects are minimized, we can expect that quantum tunneling and the associated quantum annealing effects to be dominant. We probe this by using a transverse field to tune the rate of quantum tunneling and thus the strength of the quantum annealing process. The basic approach is illustrated in Figs. 5 A&B. First, consider three subsystem states, 1, 2 and 3 which, for a bath characterized by the temperature-dependent parameter $\alpha(T)$, exchange places in their ranking according to the classical potential energy as T is lowered to yield $\alpha(T) = \alpha_1, \alpha_2, \alpha_3$. This potential energy is defined by other degrees of freedom which may be undergoing thermal fluctuations that are slow on the scale of the tunneling times for the three levels being considered. We now introduce quantum mixing, in this case via a transverse magnetic field. The potential energy curves are drawn so

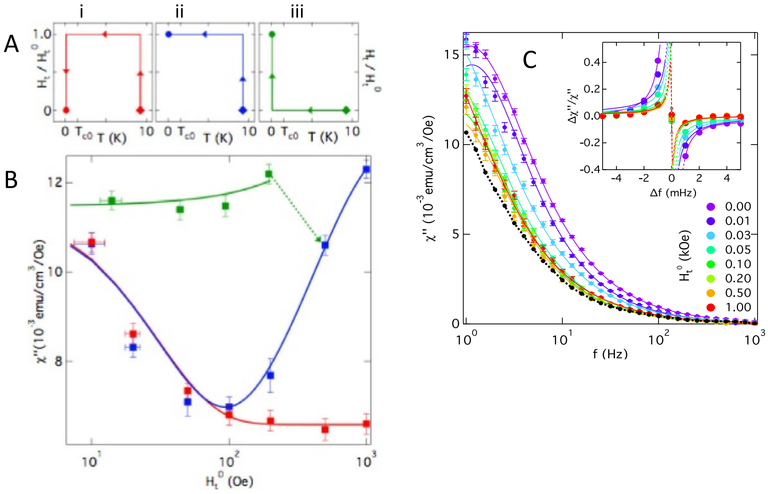

Fig. 6. Quantum annealing in LiHo$_{0.045}$Y$_{0.955}$F$_4$. (Ref. [8]) A) Trajectories through $H_t - T$ space. B) Constant-frequency response of the imaginary part of the susceptibility following the three different cooling trajectories over a range of transverse fields. In the quantum annealing trajectory (i), as in (ii), where the quantum fluctuation rate remains constant approaching the final state, $H_t^0 \sim 0.1$ kOe demarcates different response regimes. The classical annealing trajectory (iii) shows a weak quantum speedup at low fields followed by an instability at fields above 0.5 kOe that yields a tunneling transition to branch (ii) with a timescale ~ 1 d. C) Imaginary part of the susceptibility from 1 Hz to 1 kHz after quantum annealing in a series of transverse fields with the crystal weakly coupled to the bath. The curve in black is the dissipative response of the sample in the strongly coupled limit with $H_t^0 = 0$. An in situ GaAs Hall magnetometer was used to directly measure the applied transverse field. (Inset) Nonlinear pump-probe spectroscopy for the same quantum annealing trajectories as in the main panel, with a 19.95 Hz/0.3 Oe pump field. Fits to a Fano resonance form (smooth curves) indicates interference between excitations of discrete spin cluster states and those in the bath; dashed lines show predicted behavior for the resonances for Δf less than the experimental resolution.

that the minima for states 1 and 2 are closer in phase space to each other than to the minimum for state 3, meaning that within a barrier tunneling picture there will be more mixing of states 1 and 2 than of either of these states with state 3. In such a circumstance, quantum mixing actually can lead to a condition where at α_3 the subsystem state will be predominantly a mixture of states 1 and 2 (blue circle) even while classically the system will clearly be in state 3 (red circle). Quantum mixing will yield such a result depending on whether the cooling rate is faster than the decoherence rate produced by the environment not incorporated in the Hamiltonian, including the mixing terms.

Figure 5C shows the experimental results for the linear susceptibility after cooling in the presence of a range of transverse fields, corresponding to a range of quantum tunneling rates. We see a softening of the spectrum as H_t is raised from zero to 100 Oe, and then a hardening upon further increasing H_t to 2000 Oe. Consistent with classical pinning, the initial softening effect is visible only when cooling in field from high temperature, whereas the high transverse field (2 kOe) hardening is history-independent and therefore consistent with H_t-induced quantum speedup.

We directly compare the end results of a classical vs. a quantum annealing trajectory for LiHo$_{0.045}$Y$_{0.955}$F$_4$ in Fig. 6. The trajectories followed are outlined in Fig. 6A. In addition to the quantum annealing protocol (i), we also followed the mixed

H_t/thermal trajectory (ii) where the transverse field H_t^0 is applied before cooling, but not removed at lowest T as in (i), and (iii) where the transverse field is only applied after cooling to the lowest T. Despite the data being collected at identical (T, H_t^0), the spectra do not coincide below $H_t^0 \sim 500\,\mathrm{Oe}$, again indicating the approach to different end states. The classical pathway (iii) becomes unstable over the course of a day for $H_t^0 \sim 500\,\mathrm{Oe}$, and the two protocols merge over repeated measurements of the spectrum. Above this field scale, the transverse field is large enough to produce the quantum fluctuations required to overcome pinning of spin configurations in the search for equilibrium. For even larger transverse fields ($H_t > 3.5\,\mathrm{kOe}$), the physics of quantum level crossings for single ions and pairs of ions emerges, where the nuclear hyperfine interaction must be considered.

An important feature of the data in Fig. 6 is that tuning the system state with H_t^0 requires thermal cycling above $T = 9\,\mathrm{K}$ before changing the transverse field. Warming above the Curie temperature of the pure compound, $T_C = 1.53\,\mathrm{K}$, or even to $T = 4\,\mathrm{K}$, is not sufficient to reset the system upon cooling. Rather, the low temperature state only responds to a change in H_t^0 if the spins are thermally excited above the $9.4\,\mathrm{K}$ splitting between the Ising ground state doublet and the first excited state singlet. This points once again to the fundamental quantum nature of the ground state when isolated from the incoherent thermal bath.

We show in Fig. 6C the spectral characteristics of the weakly coupled spins after quantum annealing. There appear to be a continuous set of low temperature states that the system can access depending on the strength of the cooling field. For $H_t^0 < 0.1\,\mathrm{kOe}$, we see that χ'' behaves as in Fig. 5C, where the cooling field was maintained to achieve the final state. In particular, there is a softening with increasing transverse field, corresponding to the random fields present on the cool-down which pin the spin configuration even after the transverse field is shut off at low T. On the other hand, the final state is much less dependent on $H_t^0 > 0.1\,\mathrm{kOe}$, consistent with the capability of quantum annealing to produce approximately the same final state independent of the exact application of the transverse field during cooling. The discrepancies found at low frequencies may be linked to small differences in precisely how the random field regime for $H_t < 0.1\,\mathrm{kOe}$ was traversed.

In summary, we have used a model magnetic system, $\mathrm{LiHo}_x\mathrm{Y}_{1-x}\mathrm{F}_4$, to test the effects of quantum annealing. This dilute alloy family combines macroscopic numbers of spins with a straightforward laboratory method for tuning the rate of quantum tunneling, and hence is a valuable substrate for studying the role of quantum annealing in equilibrating systems with complex energy landscapes. Examining two members of the $\mathrm{Li(Ho,Y)F}_4$ family, one with a dense collection of spins and the possibility of a long-range ordered state, and one with a sparser spin density in which glass dynamics and quantum fluctuations dominate the behavior, we find in both cases that reaching equilibrium through a quantum annealing trajectory produces a different end state than a purely thermal annealing approach. In examining the more dilute case, we find that the coupling to the thermal bath can be manipulated to actually engineer the quantum character of a bulk spin system.

References

1. P. Ray, B.K. Chakrabarti, A. Chakrabarti, Phys. Rev. B **39**, 11828 (1989)
2. E. Farhi, J. Goldstone, S. Gutmann, J. Lapan, A. Lundgren, D. Preda, Science **292**, 472 (2001)
3. G.E. Santoro, R. Martonak, E. Tosatti, R. Car, Science **295**, 2427 (2002)
4. A. Das, B.K. Chakrabarti, Rev. Mod. Phys. **80**, 1061 (2008)
5. M.W. Johnson, et al., Nature **473**, 194 (2011)
6. J. Brooke, D. Bitko, T.F. Rosenbaum, G. Aeppli, Science **284**, 779 (1999)

7. J. Brooke, T.F. Rosenbaum, G. Aeppli, Nature **413**, 610 (2001)
8. M.A. Schmidt, D.M. Silevitch, G. Aeppli, T.F. Rosenbaum, Proc. Natl. Acad. Sci **111**, 3689 (2014)
9. S. Boixo, T.F. Rønnow, S.V. Isakov, Z. Wang, D. Wecker, D.A. Lidar, J.M. Martinis, M. Troyer, Nature Phys. **10**, 218 (2014)
10. P. Beauvillain, J. Renard, I. Laursen, P. Walker, Phys. Rev. B **18**, 3360 (1978)
11. P. Chakraborty, P. Henelius, H. Kjonsberg, A. Sandvik, S. Girvin, Phys. Rev. B **70**, 144411 (2004)
12. P. Hansen, T. Johansson, R. Nevald, Phys. Rev. B **12**, 5315 (1975)
13. W. Wu, B. Ellman, T.F. Rosenbaum, G. Aeppli, D.H. Reich, Phys. Rev. Lett. **67**, 2076 (1991)
14. D. Bitko, T.F. Rosenbaum, G. Aeppli, Phys. Rev. Lett. **77**, 940 (1996)
15. D.M. Silevitch, D. Bitko, J. Brooke, S. Ghosh, G. Aeppli, T.F. Rosenbaum, Nature **448**, 567 (2007)
16. D.H. Reich, B. Ellman, J. Yang, T.F. Rosenbaum, G. Aeppli, Phys. Rev. B **42**, 4631 (1990)
17. S.M.A. Tabei, M.J.P. Gingras, Y.-J. Kao, P. Stasiak, J.-Y. Fortin, Phys. Rev. Lett. **97**, 237203 (2006)
18. M. Schechter, Phys. Rev. B **77**, 020401 (2008)
19. J.A. Quilliam, S. Meng, C.G.A. Mugford, J.B. Kycia, Phys. Rev. Lett. **101**, 187204 (2006)
20. S. Ghosh, R. Parthasarathy, T.F. Rosenbaum, G. Aeppli, Science **296**, 2195 (2002)
21. R. Giraud, W. Wernsdorfer, A. Tkachuk, D. Mailly, B. Barbara, Phys. Rev. Lett. **87**, 057203 (2001)
22. R. Giraud, A.M. Tkachuk, B. Barbara, Phys. Rev. Lett. **91**, 257204 (2003)